RESEARCH ARTICLE

Key Points:
- Lagrangian dispersion cannot be addressed on mean velocity fields only
- Interannual variability of dispersion is very high
- Kinematic modeling helps to describe the small-scale dispersion

Supporting Information:
- README file for Supplementary Materials
- Supplementary Movies

Correspondence to:
L. Palatella,
luigi.palatella@yahoo.it

Lagrangian simulations and interannual variability of anchovy egg and larva dispersal in the Sicily Channel

Luigi Palatella[1,2], Francesco Bignami[3], Federico Falcini[3], Guglielmo Lacorata[1], Alessandra S. Lanotte[1,2], and Rosalia Santoleri[3]

[1]Istituto di Scienze dell'Atmosfera e del Clima, Consiglio Nazionale delle Ricerche, Lecce, Italy, [2]Istituto Nazionale di Fisica Nucleare, Sezione di Lecce, Lecce, Italy, [3]Istituto di Scienze dell'Atmosfera e del Clima, Consiglio Nazionale delle Ricerche, Roma, Italy

Abstract The interannual variability in the transport of anchovy eggs and larvae in the Sicily Channel, relatively to the period 1999–2012, is studied by means of numerical simulations of the Mediterranean Forecasting System (MFS) circulation model provided by INGV. Subgrid-scale dynamics not resolved by the MFS model is parameterized in terms of kinematic fields. The latter affect small-scale tracer relative dispersion, while leaving the mean large-scale advection substantially unchanged. A Lagrangian Transport Index (LTI) can be defined to characterize the efficiency of the main currents, e.g., the Atlantic Ionian Stream, in connecting spawning and nursery areas to each other. In our case, this indicator comes from the first arrival time statistics of tracers traveling from a spawning area near Sciacca to a nursery area in proximity of Cape Passero. We observe, on the basis of LTI values, that there are years when the Lagrangian connectivity is very efficient (2004, 2008, 2012) and years when it is weak (2000, 2001, 2003, 2010). Lagrangian indicators like the LTI concur to explain observed fluctuations of larval density and, also, can be employed, more in general, in multivariate models of population dynamics.

1. Introduction

The Sicily Channel (also called Strait of Sicily) represents an important area of the Mediterranean Sea because of its fundamental role in linking the western and eastern Mediterranean subbasins [*Malanotte-Rizzoli and Robinson*, 1994]. Beyond oceanographic aspects, this Channel also represents a crucial geographic spot, being the narrowest channel (except the Gibraltar Strait) that separates north Africa from Europe, and the set course for commercial shipping directed to and coming from Eastern and Western Europe, as well as the Middle East. From a socio-economical perspective, moreover, the Sicily Channel is one of the main fishing sites in the Mediterranean, and represents a particularly appropriate region for investigating those kinds of features that relate ocean dynamics to egg spawning and egg and larva transport properties, as well as fish landings [*Garcia-Lafuente et al.*, 2002].

The surface circulation through the Channel, see Figure 1, is mainly characterized by an along channel, meandering current of Atlantic origin, the Atlantic Ionian Stream (AIS) [*Robinson et al.*, 1999]. The AIS climatologically encircles two cyclonic vortices over the Adventure Bank and off Cape Passero, i.e., the Adventure Bank Vortex (ABV) [*Lermusiaux*, 1999; *Robinson et al.*, 1999; *Lermusiaux and Robinson*, 2001] and the Ionian Shelf Break Vortex (IBV), respectively, and describes a pronounced anticyclonic meander in between (i.e., the Maltese Channel Crest, MCC). A third cyclonic vortex—the Messina Rise Vortex (MRV)—is sometimes found on the eastern side of Sicily, south of Messina strait [*Lermusiaux*, 1999].

The southern and southwest portion of the Channel is invested by the Atlantic Tunisian Current (ATC), which climatologically flows along the Tunisian coasts as a second, southeastward branch of Atlantic water.

All the hydrological features above described are generally recognized by the Sea Surface Temperature (SST, Figure 1) that well marks differences among the sea surface structures, especially during conditions of summer high thermal stratification.

In addition to the climatological, large-scale sea surface circulation in the Sicily Channel, whose spatial pattern is mainly related to the interaction between hydrological properties and the Channel topography [*Sorgente et al.*, 2011], Lagrangian experiments carried out during the 1990s [*Poulain and Zambianchi*, 2007]
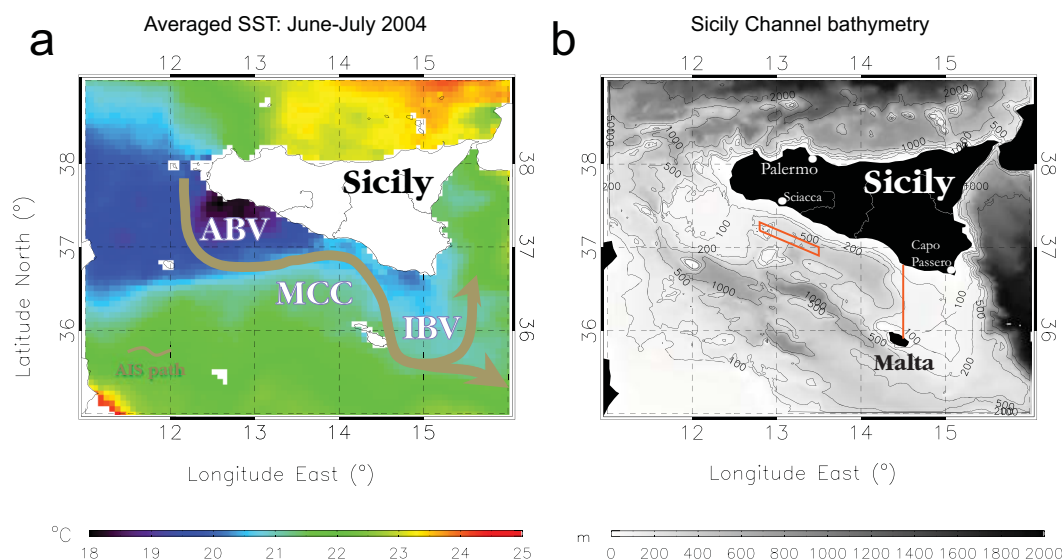
Figure 1. (a) The study area we have considered: Southern Mediterranean, Sicily Channel. Here the Atlantic Ionian Stream, with its spatial and temporal variability, is the major dynamical mechanism of transport in that region. The sea surface temperature satellite data map refers to the average over June–July 2004. (b) The spawning area, assumed to be located near Sciacca, is plotted in the map; the larvae recruitment area is near Cape Passero. The region east of the vertical line is considered as the target area in the Lagrangian numerical simulations performed.

revealed an important seasonal variability, mostly due to the wind forcing. During summer, the AIS is particularly strong on the Sicilian side of the Channel, while the ATC appears to be weaker; in winter periods, the ATC is characterized by a strong signature, surface currents in the central region of the Channel are weak or reversed (heading northwestward), and the meandering feature of the AIS is weakened, resulting in a confinement of this water along the Sicilian coast.

Although the main dynamical features of the Sicily Channel are determined by the large-scale circulation systems above described, transport and diffusion properties cannot be deduced from the knowledge of climatological mean currents alone, since the presence of chaotic behavior in the evolution of Lagrangian trajectories may drastically change the picture [*Ottino*, 1989]. Lagrangian chaos [*Crisanti et al.*, 1991] is the major physical mechanism of tracer dispersion that can be observed even in nonturbulent flows. Moreover, it determines a substantial separation between the stability properties of the velocity field and the unstable dynamical evolution of the fluid particle trajectories (i.e., sensitivity to initial conditions). For a time-dependent meandering jet-like flow, such as the AIS, it is not obvious to estimate the mean transport along and across the stream [*Poulain and Zambianchi*, 2007]. Lagrangian trajectories may display very irregular, chaotic behaviors due to the time-dependent components of the dynamical system. In particular, an open streamline region (jet) can be affected by cross-stream dispersion that removes particles from the main path and, conversely, a closed streamline region (vortex) can lose material across the boundaries by chaotic diffusion. This may occur in a purely deterministic, nonlinear velocity field, without adding any small-scale noise component to the dynamics [*Crisanti et al.*, 1991].

In this work, we investigate, statistically, Lagrangian transport in the Sicily Channel, and its interannual variability. We also explore how our results are affected by the introduction of two and three-dimensional sub-grid-scale (SGS) Lagrangian models, describing space and time fluctuations otherwise unresolved by large-scale circulation models. As Lagrangian tracers we will consider eggs and larvae of the European Anchovy (*Engraulis encrasicolus*, Linnaeus, 1758). This commercial species represents one of the most important resources of the Mediterranean Sea and its distribution properties along the Sicily Channel are still poorly understood [*Cuttitta et al.*, 2003; *Garcia-Lafuente et al.*, 2002]. We therefore propose a Lagrangian approach [*LaCasce*, 2008] as a first step toward a better understanding of the relationship between anchovy population and sea surface dynamics. This work offers a contribution to the study of Lagrangian connectivity [*Cowen et al.*, 2000] between spawning and nursery areas. More specifically, we seek to quantify the amount of larvae coming from a certain spawning region that are able to reach a particular nursery region. The Lagrangian models make use of the Eulerian velocity field provided by the Mediterranean Forecasting

System-MFS [*Oddo et al.*, 2009; *Dobricic and Pinardi*, 2008] model analysis. We are aware that an important limitation for biological applications is the fact that the model resolution does not allow to release particles too close to the coasts, while spawning and nursery areas are indeed quite coastal. So necessarily we have to adopt some kind of approximation in the choice of the initial conditions.

The paper is organized as follows: in section 2., we introduce the large-scale ocean circulation model and the subgrid-scale parameterizations. In section 3., we describe the numerical setup of the different models. Next, we describe, in section 4., the results of our Lagrangian simulations of anchovy eggs and larvae trajectories for the Sicily Channel, while an idealized case of a meandering jet conceptually similar to the Atlantic-Ionian Stream is presented in Appendix B. This is done to highlight the strong influence of Lagrangian chaos on particle transport. Section 4. results include a sensitivity test for the Sicily Channel obtained by changing some of the different parameters present in the models. This test can be regarded as an initial validation effort, together with the analysis of the error growth between model trajectories and that of an in situ drifter, given in Appendix A. Our intention is to pursue the validation effort in the future, e.g., by comparison with the output of eddy-resolving higher resolution circulation models. Finally, in section 5., the above results relatively to the Channel of Sicily are discussed, also, in the perspective of the applicability of the present model setup to other basins.

2. Lagrangian Modeling of the Central Mediterranean Region

2.1. Large-Scale Circulation Fields and the Atlantic Ionian Stream

We now consider the velocity fields describing the dynamics of the Central Mediterranean Sea. Zonal (u_{MFS}) and meridional (v_{MFS}) components of the velocity are provided by the Mediterranean Sea Forecasting System model Analysis fields (hereafter MFS) [*Tonani et al.*, 2008; *Oddo et al.*, 2009], which is now part of the MyOcean Project operational oceanography modeling effort (http://gnoo.bo.ingv.it/mfs/myocean/description.html). The Mediterranean Forecasting System [*Dobricic and Pinardi*, 2008; *Oddo et al.*, 2009] produces every day a 10 day current and temperature forecast for the Mediterranean Sea and analyses every 7 days. MFS adopts spherical coordinates and the Boussinesq, hydrostatic, and incompressible approximations and is forced with surface fluxes derived from ECMWF fields. Horizontal and vertical resolutions are: $1/16° \times 1/16°$ degrees ($\simeq 6.5$km) and 72 vertical levels (which go from 1.5 to 5000 m depth), respectively. Vertical levels are unevenly spaced and have a thickness ranging from 3 m at the surface to 300 m at the bottom. Since the first internal Rossby radius of deformation for the Sicily Channel region is typically of the order O(10) km [see *Grilli and Pinardi*, 1998], the model is not eddy resolving but only eddy permitting. In the MFS model, the horizontal eddy viscosity and eddy diffusivity are taken as constant, and equal to $5 \times 10^9 \text{m}^4/\text{s}$ and $3 \times 10^9 \text{m}^4/\text{s}$, respectively, where dissipative terms are bi-Laplacian. Vertical diffusivity and viscosity are both a function of the Richardson number [see *Tonani et al.*, 2008], and these parameterizations are thought to work satisfactorily as far as mixed-layer processes are concerned. MFS assimilates satellite (sea level anomaly, SST) and in situ (ship or drifter temperature and salinity profiles) data with the 3DVar scheme [*Dobricic and Pinardi*, 2008].

The MFS analyses quality has been assessed for the past 10 years by comparing temperature, salinity, and sea level analysis fields with in situ and satellite observations [*Tonani et al.*, 2009] (see also http://gnoo.bo.ingv.it/mfs/myocean/evaluation.html). The results show that in the surface layer the temperature is accurate with a RMS error always below 1°C, while the salinity is consistent with the observation even if the error is higher in the first 10 m but always with a RMS less than 0.4 psu. Compared with satellite-derived sea level data, the MFS reproduces similar energy spectra [*Oddo et al.*, 2009]. Recently, *Marullo et al.* [2013] analyzed the spectral characteristics of the model surface field and showed that the model correctly reproduce the spectra and amount of energy of the in situ surface field for frequencies lower than 24 h. As regards specifically to Lagrangian motion, we present a preliminary analysis on the discrepancy between model and drifter data in Appendix A.

Since we focus on transport and dispersion properties during the anchovy spawning season in the Sicily Channel, we consider daily snapshots of the velocity fields that cover the months from June to September, for the period 1999–2012. In particular, we investigate how the AIS influences the larval transport in the Channel, given its space-time variability. As an example, in Figure 2, we plot, for two reference periods, June 2004 and June 2011, maps of the kinetic energy (per unit mass) associated to the mean velocity field and to
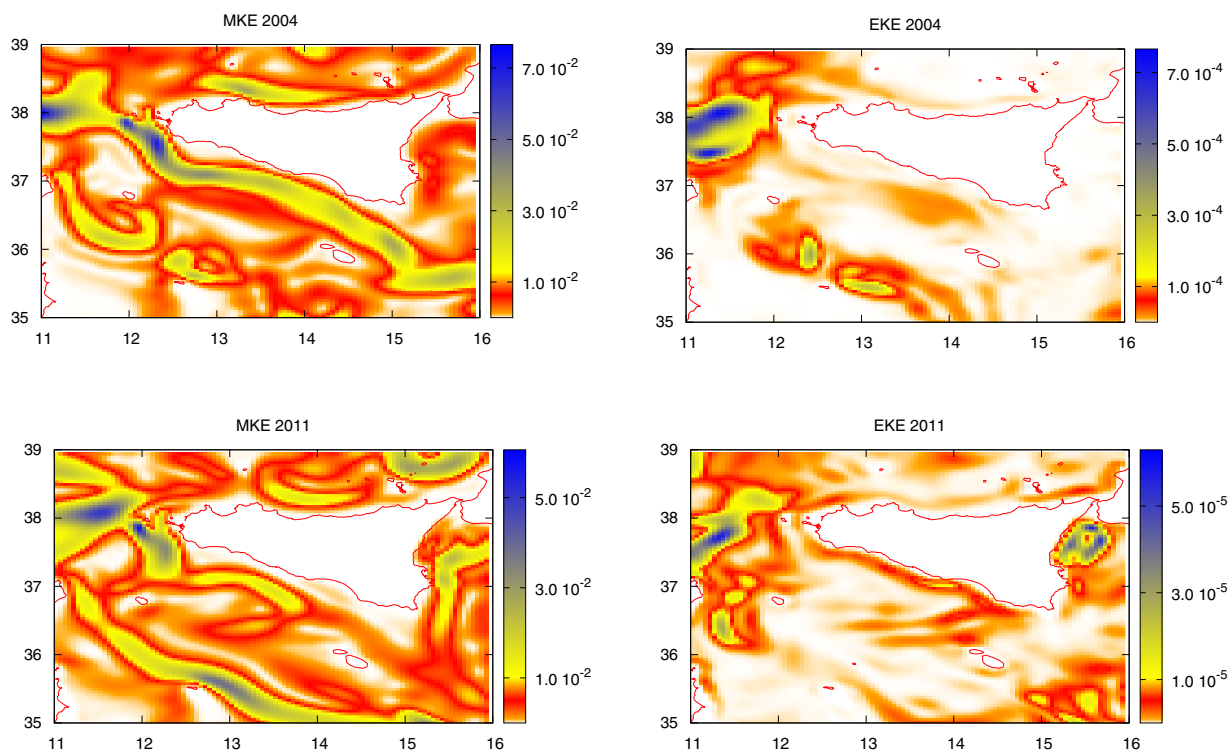
Figure 2. Maps of Kinetic Energy (per unit mass) associated to the mean velocity field (MKE) and to the velocity field fluctuations (EKE), for June 2004 and June 2011. Data are measured at $z = -20$m depth. Kinetic energy is measured in $m^2 s^{-2}$.

the velocity field fluctuations (with respect to the mean) at about $z \simeq -20$m, i.e., within the mixed layer, where the AIS signal is strong. The kinetic energy associated to the mean field shows the clear signature of the AIS, close to the coast in 2004, and well offshore around $35°$ latitude in 2011. The AIS shows a mean current amplitude of the order of 0.5 m/s an its position is generally different from 1 year to another. Furthermore, surface layers are generally affected by strong daily variability which is wind induced, while deeper layers are clearly more stationary.

All this suggests that caution is needed when one tries to extract Lagrangian transport properties from long-time averages of the Eulerian velocity field [*Poulain and Zambianchi*, 2007].

In the MFS model, the high wave number variability is often lost because of the smoothing operations, also associated with time averaging. Moreover, daily snapshots are of course unable to describe the high-frequency variability—with characteristic times smaller than $O(1)$ day—of the marine currents.

As discussed in the following, a SGS field with eddies of size of the order of the Rossby radius ($\sim O(10)$km for the Mediterranean Sea), and characteristic turnover times of order $O(1)$ day or less, provides a way to restore, although only partially, the short time and small-scale variability of the transport process.

In Appendix B, we consider a simplified jet stream model as test case in which it is clearly shown how Lagrangian transport properties can be sensitive to the time variability of the large-scale nonlinear Eulerian structures.

2.2. Subgrid-Scale Kinematic Fields

Unresolved motions on subgrid scales in a general circulation model can be described by adopting various techniques, from stochastic differential equations that simulate turbulent diffusion and dispersion by means of suitable Markov processes [*Sawford*, 2001; *Brickman and Smith*, 2002], to deterministic kinematic fields that exploit Lagrangian chaos as primary mechanism of tracer dispersion. This second approach is the one we adopted in this work, for a number of reasons: deterministic flows simulated by chaotical systems (i) may supply coherent structures (jets, eddies) and, consequently, spatial correlations that are difficult to

reproduce within stochastic models; (ii) allow for exponential separation of trajectories, even at finite scales; and (iii) kinematic fields of the type discussed in this work are incompressible by definition.

Broadly speaking, there are two main issues related to the simulation of transport and mixing of particles in an ocean circulation model: (i) the lack of resolution of submesoscale horizontal motions and (ii) the underestimation of the vertical mixing in the upper layer. In the approach here adopted, each of these instances requires a different treatment. A 2-D SGS field is introduced for the former case, that mainly accounts for dispersion by structures of the size of the Rossby radius; a 3-D field is introduced, that mimics the action of small-scale eddies of few meters size, typical of the oceanic mixing layer.

The 2-D kinematic velocity field is a time-dependent flow of the type

$$
\begin{aligned}
u &= A \sin[k(x - \varepsilon \sin(\omega t))] \cos[k(y - \varepsilon \sin(\omega t))], \\
v &= -A \cos[k(x - \varepsilon \sin(\omega t))] \sin[k(y - \varepsilon \sin(\omega t))],
\end{aligned}
\tag{1}
$$

derived from a stream function of the form

$$
\Psi = \frac{A}{k} \sin[k(x - \varepsilon \sin(\omega t))] \sin[k(y - \varepsilon \sin(\omega t))].
\tag{2}
$$

according to the Hamiltonian formalism established by definition (B2). Hence, the divergence of the field of equation (1) is necessarily null.

In equations (1) and (2), A is the maximum attainable velocity (the same for both directions in order to guarantee isotropy of the dispersion process); $k = 2\pi/l_0$ is the spatial wave number associated to the spatial wavelength l_0; ε is the maximum oscillation amplitude; T_p is the period; and $\omega = 2\pi/T_p$ is the pulsation of the perturbation. The velocity field in (1) is a lattice of nonsteady convective cells [*Solomon and Gollub*, 1988; *Crisanti et al.*, 1991], of size $l_0/2$ and eddy-turnover time of the order $t_c \sim l_0/A$, subject to time-periodic oscillations around their mean positions. Of course, a single 2-D eddy wavelength and a homogeneous 2-D eddy field are a crude starting point approximation. However, the Sicily Channel is seen to have a quite ubiquitous eddy field, as results by high-resolution model simulation [e.g., *Napolitano et al.*, 2003; *Sorgente et al.*, 2011] and by the analysis of satellite data [*Ciappa*, 2009; *Buongiorno Nardelli et al.*, 2003]. This reasonably justifies our approach, which considers a homogeneous eddy field for Lagrangian simulations.

When $\varepsilon = 0$, the flow is steady and particle trajectories follow closed orbits within a convective cell. When Lagrangian chaos is turned on, for typical parameter values $\omega \sim 1/t_c$ and $\varepsilon \sim 10^{-1}l_0$, the trajectories become nonperiodic orbits and large-scale dispersion takes place.

In an ocean circulation model, with spatial resolution of order $\sim O(1-10)\text{km}$ and daily-averaged velocity fields, a flow of the type (1) can be used as submesoscale model, with $l_0/2$ of the order of the Rossby radius of deformation and $t_c \sim O(1)$ day. The idea is to restore, from a Lagrangian point of view, the dispersion rate of trajectories at scales not resolved by the ocean circulation model. As mentioned above, to account for small-scale vertical mixing a 3-D lattice of convective cells can be introduced. Here we adapt the model introduced in *Lacorata et al.* [2008] to our oceanic context. This model simulates chaotic Langmuir cell-like vertical convection and is adopted because often such a vertical mixing process overwhelms the action of the small-scale turbulence. We define an incompressible 3-D velocity field of components (u, v, w), as the curl of a potential vector Φ, of components $(\Phi_1, \Phi_2, 0)$ given by

$$
\begin{aligned}
\Phi_1 &= A\hat{k} \sin[k(x - \varepsilon \sin(\omega t))] \sin[\hat{k}(z - \varepsilon \sin(\omega t))], \\
\Phi_2 &= A\hat{k} \sin[k(y - \varepsilon \sin(\omega t))] \sin[\hat{k}(z - \varepsilon \sin(\omega t))],
\end{aligned}
\tag{3}
$$

where A is the velocity scale, $k = 2\pi/\lambda_0$ is the horizontal wave number associated to the wavelength λ_0 of the flow, $\hat{k} = 2k$ is the vertical wave number assumed to be twice the horizontal wave number for isotropy, $t_c = \lambda_0/A$ is the convective time scale; ε and ω are amplitude and pulsation of the time-dependent oscillating terms.

To account for the suppression of vertical convection below the mixed layer, both stream functions Φ_1 and Φ_2 in (3) can be multiplied by a damping term, e.g., $\Upsilon(z) = e^{-|z|/\eta}$, which relaxes exponentially to zero at depths z much larger than η, where η is a length scale of the order of the mixed layer depth.

By definition, the three components of the velocity field are

$$u = \frac{\partial \Phi_1}{\partial z}, \quad v = -\frac{\partial \Phi_2}{\partial z}, \quad w = -\frac{\partial \Phi_1}{\partial x} + \frac{\partial \Phi_2}{\partial y}, \tag{4}$$

for which we necessarily have $\partial u/\partial x + \partial v/\partial y + \partial w/\partial z \equiv 0$. The parameters of the time-dependent terms have the typical setup $\varepsilon/\lambda_0 \sim O(10^{-1})$ and $\omega \cdot t_c \sim O(1)$. In this case also, Lagrangian chaos is the mechanism that generates large-scale trajectory dispersion, as far as the time-dependent terms in the velocity field are turned on.

If one is interested in simulating motions due to multiple eddies over a range of scales, it can be convenient to consider the superposition of a series of N_m spatial modes:

$$\Phi_1 = \sum_{n=1}^{N_m} \Phi_1^{(n)}, \quad \Phi_2 = \sum_{n=1}^{N_m} \Phi_2^{(n)}, \tag{5}$$

where $\Phi_1^{(n)}$ and $\Phi_2^{(n)}$ have the same analytical form of equation (3). The velocity scale A_n, the wave numbers k_n (horizontal) and $\hat{k}_n$ (vertical), the oscillation amplitudes ε_n, and pulsations ω_n are parameters that now depend on the nth mode. Since we are interested in simulating chaotic vertical dispersion in the mixed layer, we use equation (5) with only two modes, with no need of including a whole inertial range of turbulent scales.

Let us indicate with $\mathbf{r} \equiv \{x, y, z\}$, the vector position of a tracer particle, and let $\mathbf{V}_{\text{MFS}} \equiv \{u_{\text{MFS}}, v_{\text{MFS}}, 0\}$, $\mathbf{V}_{\text{2D}} \equiv \{u_{\text{2D}}, v_{\text{2D}}, 0\}$, and $\mathbf{V}_{\text{3D}} \equiv \{u_{\text{3D}}, v_{\text{3D}}, w_{\text{3D}}\}$ be the velocity fields given by the MFS, 2-D SGS, and 3-D SGS models, respectively. The equation system for the time evolution of Lagrangian tracer particles is then

$$\frac{d\mathbf{r}(t)}{dt} = \mathbf{V}_{\text{MFS}}(\mathbf{r}, t) + \mathbf{V}_{\text{2D}}(\mathbf{r}, t) + \mathbf{V}_{\text{3D}}(\mathbf{r}, t). \tag{6}$$

In the kinematic simulations, the spatial coordinates $\mathbf{r}$ appearing in the velocity fields $\mathbf{V}_{\text{2D}}$ and $\mathbf{V}_{\text{3D}}$ in (6) are replaced by relative coordinates computed in the reference frame of the mass center of two initially close particles, i.e., in the so-called Quasi-Lagrangian frame [*Boffetta et al.*, 1999; *Lacorata et al.*, 2008]. In this way, the spatial coordinates of each particle are relative to the position of the pair center of mass, which, ultimately, moves under the action of the large-scale resolved (MFS) field. The use of relative coordinates allows one to properly simulate the advection of the small-scale kinematic eddies by the large-scale ones of the resolved field.

The temporal scheme integration for the equation (6) is the fourth-order Runge-Kutta for the subgrid dynamics; the large-scale MFS field is linearly interpolated in time between two consecutive days. Spatial interpolation is performed using bicubic spline in the horizontal directions and linear interpolation between different depths. The full algorithm is implemented in C and then run on a cluster with 24 parallel processors.

3. Anchovy Egg and Larva Transport Simulation in the Sicily Channel

It is currently accepted that the AIS transports anchovy eggs and larvae toward the southernmost part of Sicily, i.e., off *Capo Passero* (Figure 1), along the frontal structure that originates from the meeting of AIS and Ionian Sea water masses [*Garcia-Lafuente et al.*, 2002]. Anchovy spawning preferably occurs where the AIS approaches the coast (i.e., around the MCC: Figure 1) [*Garcia-Lafuente et al.*, 2002]. Therefore, changes of the AIS spatial pattern can enlarge or reduce the area occupied by the cyclonic vortices, and displace the MCC zonally or/and meridionally. Because of temperature conditions, one of the most favorable local spawning zones is placed south of the city of Sciacca [*Cuttitta et al.*, 2003] (Figure 1). In this study, we perform Lagrangian numerical experiments using a set of initial positions for the eggs inside the parallelogram

with vertices (longitude E-latitude N) $(12.8^{\circ}, 37.2^{\circ})$, $(12.8^{\circ}, 37.3^{\circ})$, $(13.5^{\circ}, 36.9^{\circ})$, $(13.5^{\circ}, 37.0^{\circ})$, off Sciacca and defined in the following as spawning area. Spatial resolution of the oceanic models generally prevents an accurate reproduction of coastal flow (within 1–2 km off the coast). Hence, to avoid numerical inaccuracy in the vicinity of domain boundaries along the coasts, our spawning area is displaced slightly offshore with respect to the actual spawning zone as reported in literature, where the feeding conditions are optimal thanks to the presence of the Belice River estuary [*Basilone et al.*, 2013].

For statistical purposes, we skip the first few hours from the release, during which we assume that the complex surface dynamics is efficient enough to drive the eggs offshore. We set the spawning rate at $\simeq 68.5 \text{eggs/day}$, from 1 June to 15 September of each year. Recently, it has been noticed that the local maximum spawning rate is in the months of July and August [*Quinci*, 2011]. Hence, in the statistical analysis, each tracer is weighed with a Gaussian distribution centered on 31 July, with a standard deviation of 30 days, to correctly reproduce the greater spawning rate of July and August. This choice does not account for any reduction of spawning activity due to sea surface temperature variations [*Quintanilla and Garcia*, 2001; *Mazzola et al.*, 2002].

Despite Lagrangian particles here simulated (i.e., anchovy eggs and larvae) have bulk dimensions up to a few millimeters, we neglect their inertial behaviors in first approximation. Note that, however, because of shape (nonspherical object), size (inertial object), and/or specific characteristics of such individuals such as gyrotactic motility, complex features may emerge in their Lagrangian motion [*Bec et al.*, 2010; *Vincenzi*, 2013; *Durham et al.*, 2013].

Although the assumption of constant egg buoyancy during their development can be questioned [*Ospina-Alvareza et al.*, 2012b], we consider that anchovy eggs are neutrally buoyant [*Olivar et al.*, 2001]. We release the eggs at the depth of 3 m. Differently, larvae are assumed to cyclically migrate from surface water, where they tend to stay during daytime, to deep water during the night [*Ospina-Alvareza et al.*, 2012a]. To mimic diel vertical migration (DVM), we optionally use the term

$$\dot{z}(t) = -\gamma[z(t) - z_0], \tag{7}$$

in the equation of motion of the vertical position z in (6). The value of the transfer rate, $\gamma \simeq 0.1 \text{h}^{-1}$, is chosen in order to let the vertical positions of the larvae relax to a depth z_0 with reasonable velocities $(\sim O(10^{-4}) \text{m/s})$. The equilibrium depths in (7) are set as

$$z_0 = \begin{cases} -3 \text{ m from } 6 \text{ am to } 6 \text{ pm} \\ -100 \text{ m from } 6 \text{ pm to } 6 \text{ am} . \end{cases} \tag{8}$$

Given some arbitrariness in the choice of γ and z_0, we evaluate the DVM effects on the horizontal dispersion, by performing a separate set of numerical experiments, with the additional term (7) inserted in the Lagrangian equations. On the basis of empirical growth functions [*Mariani et al.*, 2010; *Palomera et al.*, 2007], we assume each individual to turn from egg to larva 1.5 days after the release, compatibly with the typical temperature measured in that marine area. Tracer trajectory stops after 25 days, since this is approximately the age at which larvae can swim fast enough to influence their horizontal motion within the current field [*Ospina-Alvareza et al.*, 2012a].

As mentioned before, the horizontal spatial resolution of the MFS fields, 6.5 km $\times$ 6.5 km, does not allow to resolve eddy variability at the internal Rossby radius scale ($\sim 10 - 20$ km) with great accuracy. To overcome this limitation, we explicitly add motions at these wavelengths in the 2-D SGS model. The influence of the 2-D SGS model on egg and larva dispersion is evaluated by the comparison with the case with only the 3-D SGS. The setup of the horizontal 2-D model, chosen accordingly to the characteristic velocities resulting from the analysis by *Poulain and Zambianchi* [2007] is

$$\begin{cases} l_0 = 20 \text{ km}, \\ A = 0.1 \text{ m/s}, \\ \omega = 2\pi A / l_0, \\ \varepsilon = 0.1 l_0. \end{cases} \tag{9}$$

With this choice, the 2-D kinematic model acts as a perturbative field, relatively to the mean advection determined by the large-scale circulation, that statistically restores part of the time variability at the Rossby scale of motion ($\sim O(10)$km) lost with the daily smoothing of the MFS fields. This model setup is compatible with experimental estimates of length and velocity characteristic scales, relatively to the Central Mediterranean, obtained by *Poulain and Zambianchi* [2007] on the basis of a large amount of Lagrangian drifter data.

As discussed above, vertical motion along z is not explicitly resolved in the MFS fields. For the scope of this work, however, a detailed knowledge of the vertical velocity field in the mixed layer is not necessary, since an efficient mixing of Lagrangian tracers can be obtained by means of chaotic convective cells [*Bees*, 1998]. For this purpose, we therefore take advantage of the 3-D SGS model described in section 2.2., for which we choose to retain only two spatial modes ($N_m=2$) in the equations (5). We fix the model parameters as follows:

$$
\begin{cases}
\lambda_1=30.0 \text{ m}; \quad \lambda_2=42.4 \text{ m}, \\
A_1=0.036 \text{ m/s}; \quad A_2=0.041 \text{ m/s}, \\
\omega_n=2\pi A_n/\lambda_n, \\
\epsilon_n=0.2\lambda_n, \\
\eta=50 \text{ m},
\end{cases}
\tag{10}
$$

with $n=\{1,2\}$. The velocity amplitudes are of the order of magnitude of experimental and numerical estimates of the vertical velocities in the ocean mixed layer [*Polton and Belcher*, 2007]. These values correspond to a dissipation rate of the order of $10^{-6}\text{m}^2\text{s}^{-3}$. The damping length η assures that, below the thermocline, vertical mixing is suppressed. Trajectories are computed with an integration time step $\tau_{in}=120$ s.

A mortality rate is also associated to eggs and larvae. In the performed runs, the survival probability $P_\alpha(t)$ of an individual is defined as

$$
P_\alpha(t)=\exp\left(-\int_0^t \alpha(t')\mathrm{d}t'\right),
\tag{11}
$$

where the mortality rate $\alpha(t)$ [*Somarakis and Nikolioudakis*, 2007; *Basilone et al.*, 2013] is given by

$$
\alpha(t)=
\begin{cases}
0.3 \text{ days}^{-1} & \text{if } t<1.5 \quad (\text{eggs}), \\
0.4 \text{ days}^{-1} & \text{if } t>1.5 \quad (\text{larvae}).
\end{cases}
\tag{12}
$$

The numerical settings here adopted do not take into full account the complex biodynamical features of egg/larva dispersal, a desirable goal that would require much more information regarding spawning areas, rates, nutrient availability, zooplankton dynamics, etc. Rather, we are interested in isolating the Lagrangian motion effects and, in particular, in identifying transport characteristics by means of a quantitative approach, i.e., the distribution of the first arrival time at the nursery area border (red line in Figure 1b) of the synthetic anchovy egg and larva particles here considered.

4. Results

We now present the results of our numerical experiments for the setup summarized in Table 1. As previously discussed, tracer dynamics is mainly dominated by the presence and by the position of the AIS. The nursery area of anchovy eggs and larvae is the region south of *Capo Passero*, i.e., the region of the Malta shelf (Figure 1). In order to evaluate the number of eggs and larvae arriving in this nursery zone, we count how many tracers cross the 14°30′E longitude meridian, in the region north of Malta (red line in Figure 1b). Indeed, during the period in exam, we recognize that all individuals passing through the channel in

Table 1. Description of the Three Model Runs Performed for June–September 1999–2012[a]

RUN	2-D	3-D	DVM
RUN A	Yes	Yes	No
RUN B	No	Yes	No
RUN C	Yes	Yes	Yes

[a]For each run (row wise), models active in tracer advection are listed with a "yes." Models include the Mediterranean Forecasting System MFS, the 2-D and 3-D SGS models and the diel vertical migration model DVM.

between Sicily and Malta reach the nursery area, while those passing south of Malta never reach it. For all tracers crossing the arrival transect (Figure 1), we compute the age of first arrival. In Figure 3, we show the histogram of the first arrival time T measured in days. The number of arriving individuals is normalized by the total number of released tracers. These data refer to RUN A, i.e., to the Lagrangian experiments where tracers are advected by the MFS fields, plus the subgrid scale contributions of both the 2-D and the 3-D models. Moreover, the mortality rate is included, while vertical
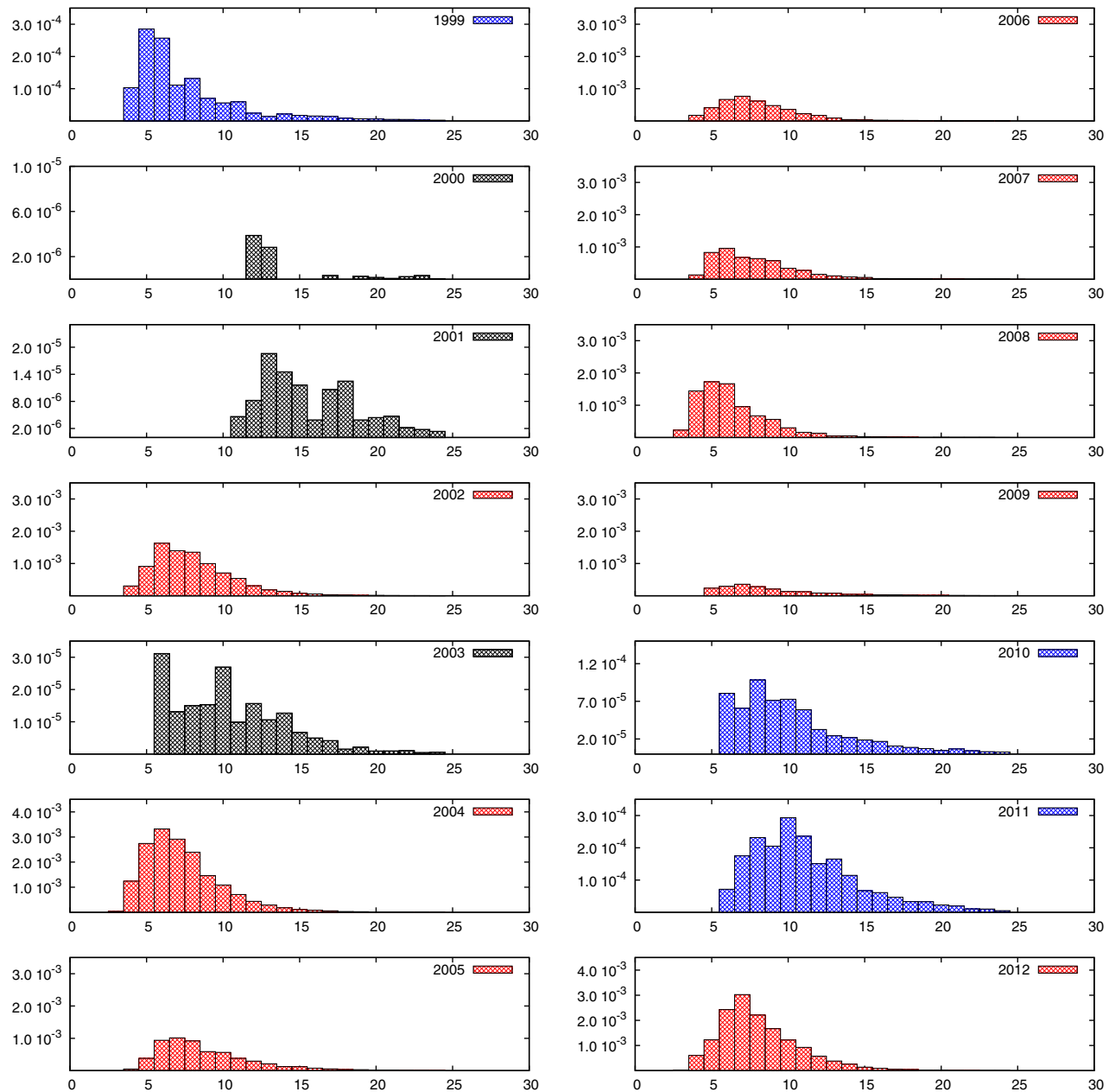
Figure 3. Statistical distributions $N(\tau)$ (y axis) of the first arrival time (x axis in days from release) of anchovy eggs and larvae, measured in terms of fraction of tracers with a given first arrival time. These results refer to numerical simulations of RUN A. Please note different ranges on y axis due to high interannual variability in $N(\tau)$.

motility is neglected. The pdfs refer to the number of tracers arrived in the selected region multiplied by the survival probability given by equation (11). The number of tracers arriving in the region, without considering the mortality rate, is significantly larger but is still a small fraction (a few percent) of the total number of the released tracers. Typically, tracers that never reach the nursery area move southward near the island of Pantelleria between Tunisia and NW Sicily (approximately 37°N, 12°E, Figure 1), and then southeastward, reaching the Ionian Sea, often entrained by the Atlantic Tunisian Current. These results display a significant annual variability both in the first arrival time and in the fraction of tracers that reach the nursery area. For the sake of clarity, we divided the first arrival time distributions in three classes of colors: red is associated to the years with the largest fraction of eggs and larvae reaching Capo Passero, i.e., $O(10^{-3})$ of the total; black is associated to years with the smallest fraction, i.e., $\leq O(10^{-5})$; and blue being the intermediate situation, i.e. $O(10^{-4})$.

Beyond the first arrival time distribution, a relevant observable is the mean or modal first arrival time in the nursery area. In the period 1999–2012, we observe that most probable first arrival times are between 5 and 6 days. Note that a longer arrival time makes the survival of the larvae quite difficult due to lack of nutrients that are mostly abundant in the nursery area [*Cuttitta et al.*, 2003].

To "disentangle" the role of the 2-D SGS model describing eddies $\sim O(10)$km large, we present in Figure 4 the first arrival time distributions from RUN B, i.e., a set of Lagrangian numerical experiments with tracers advected by the MFS fields and the 3-D SGS model only. Initial conditions are the same as in the previous experiment, as well as the postprocessing of data. As for the interannual variability of transport properties, results do not show significant qualitative differences in the two cases. However, if we compare Figures 3 and 4, we note that while the 2-D subgrid scale contribution in RUN A does not seem to change shape and magnitude of the first arrival time distributions for the "red" cases (Figure 3) with respect to no 2-D case of RUN B (Figure 4), larger relative differences are observed for "blue" and, in particular, "black" years, when the 2-D perturbation field is introduced. A further insight into the statistical properties of the Lagrangian transport model is displayed in Figure 5. Here we plot histograms of the first arrival time, for a reference year 2004 and computed in the three following cases: RUN B (with no 2-D SGS kinematic field), RUN A with the 2-D SGS field and maximum velocity amplitude $A=0.1$m/s in equation (9), and RUN A1 with the 2-D SGS field having larger maximum velocity amplitude $A=0.2$m/s. A larger amplitude of the 2-D horizontal velocity field corresponds to shorter mean arrival times of the anchovy eggs and larvae to the target area, as expected. This effect is to be considered when building up the model setup providing the best agreement with experimental data.

On the basis of the previous observations, it is clear that while the 2-D SGS model does not alter the mean advection by the large-scale modes, it helps in better describing the dispersion process on scales of the order of the Rossby radius or less.

Finally, we report the integral of the pdfs over the arrival times in order to have a single indicator dubbed as Lagrangian Transport Index (LTI), quantifying the spawning success from a dynamical point of view, with and without considering the 2-D SGS field. In Table 2, the value of LTI for the years from 1999 to 2012 is given, for the different sets of numerical simulations. To separately highlight the different effects, we have performed a third set of experiments, RUN C, where in addition to the 2-D and the 3-D SGS models, we also included the larvae vertical dynamics (i.e., DVM), according to equation (7).

Results confirm—with the exception of the years 2002 and 2009—the role of the 2-D and the 3-D SGS field in helping larva and egg transport toward the nursery area off *Capo Passero*, particularly for those years characterized by lower mean arrival times (i.e., blue and black years in Figures 3 and 4). We also note that the introduction of DVM effects does not dramatically change this scenario, since the vertical individual motility is often comparable with turbulent mixing processes.

In order to check the sensitivity of the Lagrangian transport index to the subgrid parameterization, we choose 1 year (i.e., 2006) as test case and repeat the simulations varying the setup of the 2-D and 3-D kinematic models. For the 2006, for example, we have the LTI equal to 0.41, 0.46, 0.40 for RUN A, B, C, respectively. We have considered the following variations:

1. RUN T1: 2-D SGS model consisting of four (instead of one) spatial modes, i.e., eddies with characteristic length 10, 5, 2.5, 1.25 km. Velocities are fixed according to a scaling $v(l) \sim l$, where l is the size of the eddies.
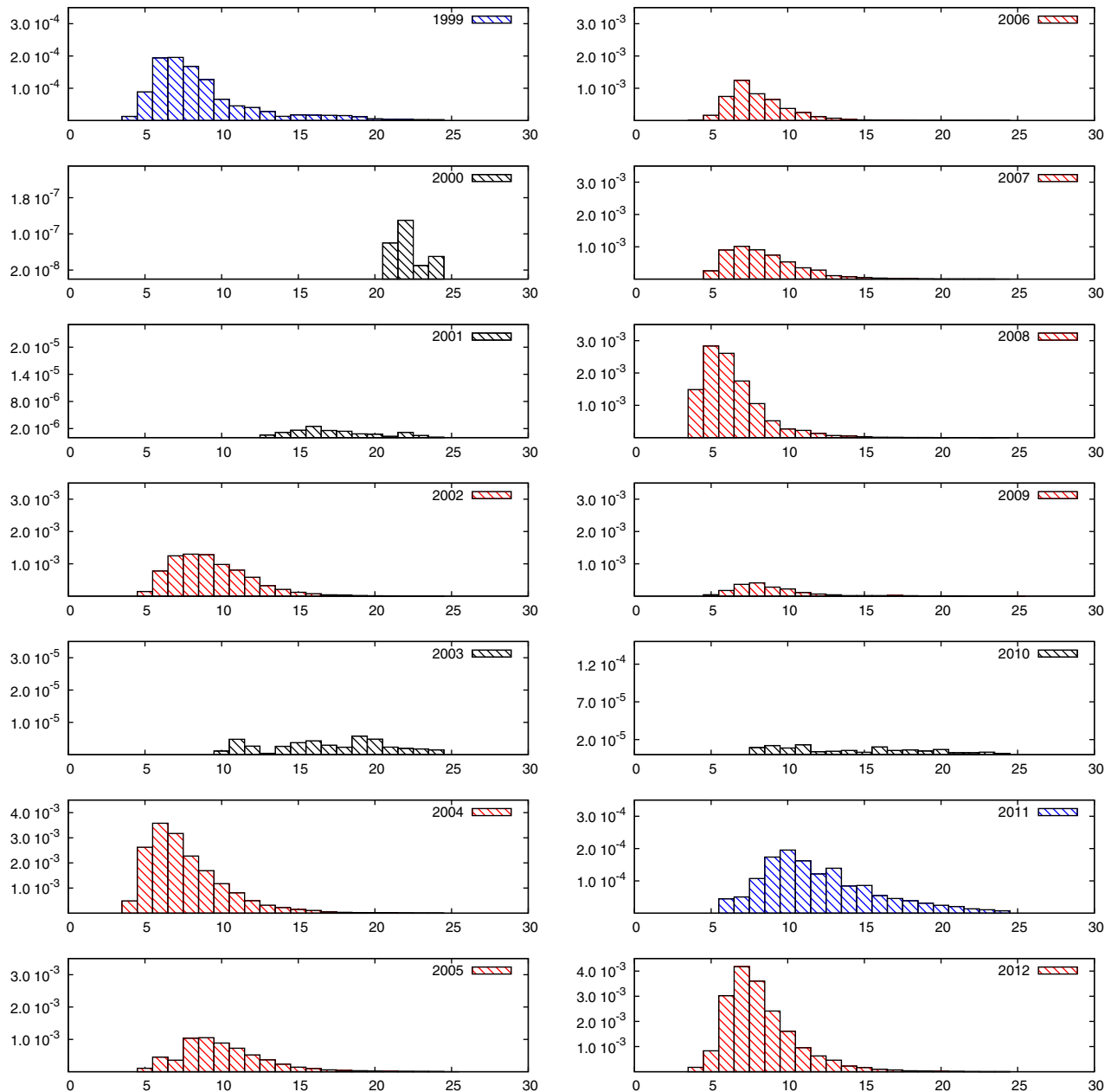
Figure 4. As in Figure 3, but for RUN B.

In this way, we have a hierarchy of cells distributed in a decade of scales, all having the same characteristic time, i.e., like in a 2-D enstrophy direct cascade [*Charney*, 1971; *Frisch*, 1995]. Velocity of the largest spatial mode (10 km) is fixed to 0.1 m/s, as for RUN A. The 3-D SGS model is the same as in RUN A and B. LTI value: 0.40.

2. RUN T2: The same setup as RUN B, but with 10 times larger ($\sim 10^{-5} m^2/s^3$) turbulent dissipation rate. LTI value: 0.35.

3. RUN T3: The same setup as T2 but with turbulent dissipation rate 10 times smaller ($\sim 10^{-7} m^2/s^3$) than the value used in RUN B. LTI value: 0.36.

4. RUN T4: The same setup as RUN B but changing the boundary conditions along the coast from beaching (RUN B) to reflection. Also, the interpolation scheme of the MFS field is changed from cubic bispline to polynomial. LTI value: 0.38.
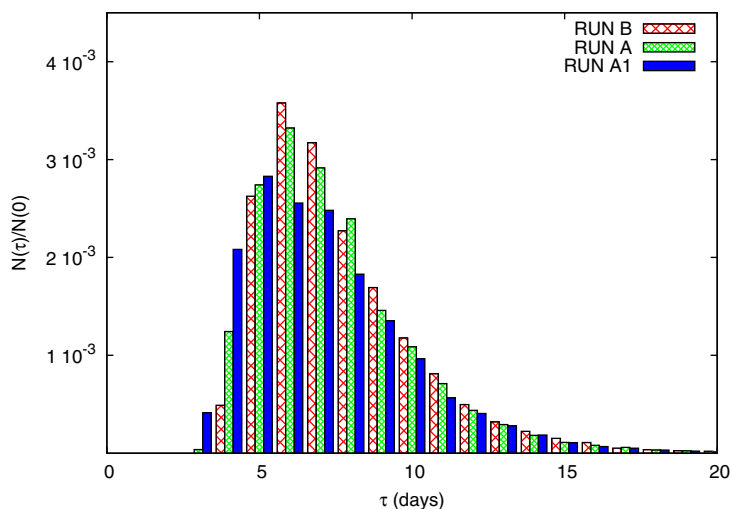
Figure 5. Histograms of 2004 first arrival times for: (red crosses) RUN B with MFS and 3-D SGS model fields; (green) RUN A with MFS, 2-D and 3-D SGS, with 2-D maximal velocity amplitude $A=0.1\text{m/s}$; and (blue) RUN A1, as for RUN A, but with $A=0.2\text{m/s}$. Higher velocities of the 2-D kinematic field determine a shorter mean arrival time.

The sensitivity test performed for the 2006 shows that the differences between the LTI of RUN A and RUN T1, and those between RUN B and RUN T2–4 are much smaller than the interannual variability (Table 2).

We can conclude that, on the basis of these sensitivity tests, the LTI values computed from the Lagrangian simulations are quite robust to large excursion of the parameters of the 2-D and 3-D subgrid fields in a wide range of values, and, moreover, to changes both in the boundary conditions and in the interpolation scheme. More sophisticated parameterizations of subgrid processes, e.g., as those introduced and discussed in *Fox-Kemper et al.* [2008], *Fox-Kemper and Ferrari* [2008], and *Fox-Kemper et al.* [2011] are not required for what concerns the kind of study presented in this work, since Lagrangian transport properties on basin scale (hundreds of km) depend very weakly on the details of the small-scale dynamics [*Crisanti et al.*, 1991, and references therein]. It only matters, in our context, that the eddy fields used to replace unresolved velocity components of the MFS model have length and time characteristic scales compatible with the physics of the system.

5. Discussion and Conclusions

In this work, we have performed numerical simulations of Lagrangian transport of anchovy eggs and larvae in the Sicily Channel. We have used the MFS model daily averaged current velocity fields as large-scale circulation model, with horizontal spatial resolution about 6.5 km × 6.5 km, into which subgrid scale (SGS) kinematic fields have been nested in order to parameterize the 2-D mesoscale and 3-D submesoscale eddy field as regular patterns of unsteady convective cells. Also a mortality rate was associated to the synthetic eggs and larvae as well as larva Diel Vertical Migration simulation (RUN C).

The above SGS kinematic models, already introduced in a study of tracer dispersion in the Planetary Boundary Layer models [*Lacorata et al.*, 2008], are an efficient numerical tool to generate chaotic and/or turbulent Lagrangian trajectories that can be adapted to various physical systems. To this regard, we would like to stress that we are modeling Lagrangian trajectory motion, not Eulerian turbulence or Eulerian dynamics in general (velocity fields, etc.). This is a point of primary importance since Lagrangian transport and diffusion properties do not depend strongly on the details of the small-scale fields. Our approach to subgrid parameterization must be considered an alternative to stochastic Lagrangian

Table 2. The Lagrangian Transport Index (LTI), i.e., the Percentage of Individuals Arriving Alive in the Recruitment Area Within 25 Days After Release, for the Three Model Runs (Table 1)

Year	LTI-RUN B	LTI-RUN A	LTI-RUN C
1999	0.11	0.12	0.11
2000	$\sim 10^{-5}$	$\sim 10^{-3}$	$\sim 10^{-3}$
2001	$\sim 10^{-3}$	0.01	0.01
2002	0.80	0.87	0.85
2003	$\sim 10^{-3}$	0.02	0.01
2004	1.73	1.72	1.48
2005	0.62	0.58	0.51
2006	0.46	0.41	0.40
2007	0.53	0.49	0.46
2008	1.11	0.80	0.73
2009	0.18	0.20	0.20
2010	0.01	0.06	0.05
2011	0.14	0.20	0.14
2012	1.85	1.49	1.32

diffusion modeling [*Sawford*, 2001], rather than to more sophisticated modeling of small-scale Eulerian processes [*Fox-Kemper and Ferrari*, 2008; *Fox-Kemper et al.*, 2008, 2011] in global climate ocean simulations.

We show the statistics of the first arrival time of anchovy larvae at the nursery region, expressed in days after release of eggs in the spawning area, both with and without subgrid 2-D parameterization. Since the difference between these two cases is measurable but small we can reasonably conclude that the outcome of a more realistic, nonhomogeneous eddy distribution (as obtained, for instance, from a high-resolution eddy-resolving model) should very likely lie in between.

A preliminary validation test of the numerical trajectories using in situ data from a single drifter is given in Appendix A. It is worth noting that the double-slope shape of the RMS error (i.e., spatial separation) growth in time between model tracer and drifter data simultaneous positions (Figure A1) suggests the presence of two characteristic times: one of the order of a few days, associated to structures of size not larger than 40–50 km that drive the initial growth of the error, and another one of the order of a few tens of days, associated to structures of large-scale size that drive the error growth at a slower rate. The RMS model-drifter error after 10 days is $O(100)$ km. Given the $O(100)$ km extension of our nursery area line and the typical arrival time of alive larvae of the order of 10 days, we think that the RMS obtained should not seriously hinder our results on the LTI, even though verification with an ensemble of drifter trajectories is probably worth to be investigated in future studies.

For the Sicily Channel, many important features of the surface circulation have been assessed by analyzing a large amount of drifter data collected in the period 1990–1999 by *Poulain and Zambianchi* [2007]. The Lagrangian integral length and characteristic time have been found to be of the order of 10–30 km and 1–2 days, respectively.

As for the Mediterranean anchovy population, furthermore, experimental information is provided by measurements of egg and larva density at fixed locations, obtained during biological surveys [see e.g., *Cuttitta et al.*, 2003]. A common assumption is that density fluctuations, in particular of eggs, are associated to a variability of the spawning area. Our Lagrangian study is focused on the effects of the interannual variability of the transport process of anchovy eggs and larvae, while keeping all the other relevant parameters fixed. From the statistics of the first arrival time from Sciacca to Cape Passero, we extract a Lagrangian Transport Index to quantify the efficiency of the marine circulation in connecting spawning and nursery areas, and to assess the interannual variability in a time span covering more than a decade.

Finally, a sensitivity test performed on year 2006 by adopting different simulation parameter values, including changes from coastal reflection to beaching of tracers and different interpolation schemes for the MFS output, suggests robustness at least for the LTI, the fraction of larvae arriving alive in the nursery area, which varies from the year 2006 between 0.35 and 0.46.

Our results suggest that, at least qualitatively, anchovy egg and larva density fluctuations can be explained in terms of Lagrangian transport variability, without invoking—but clearly not excluding—interannual variations of the spawning area and/or the spawning rate. It is worth comparing 1999–2001 egg density in situ surveys [*Cuttitta et al.*, 2003, Figures 2a–2c] with our numerical simulations of tracer transport (Palatella_et-al_movie1999-ms00.gif, _movie2000-ms01.gif and _movie2001-ms02.gif) (given in supporting information). Without altering the features of the spawning area, we observe a marked increase, during summer 2000 and 2001, in simulated egg density (red points in the movie) near Adventure Bank with respect to what is observed, for instance, during summer 1999. Hence, as far as the population dynamics of small, neutrally buoyant, passive tracers is concerned, it can be risky to draw conclusions about the transport properties on the basis of averaged fields only, since, in general, mean tracer advection does not coincide with advection by mean field.

Our approach may have applications on similar fishery studies in order to quantify, and predict larvae recruitment variability. For instance, in the Bay of Biscay [*Borja et al.*, 1998] and off the Agulhas bank in South Africa [*Hutchings et al.*, 1998] Lagrangian statistical properties, such as the LTI introduced in this paper, can be associated to anchovy recruitment variability. As another example, Lagrangian transport properties of the shelf-slope frontal system running along the Catalonian shelf [*Font et al.*, 1988] can be investigated for inferring anchovy population distribution. Nutrient and temperature distributions associated with the discharges of the Rhone and Ebro rivers, affecting larval survival potential [*Garcia and Palomera*, 1996; *Lloret et al.*, 2004] could also be a possible case study for our Lagrangian Approach.
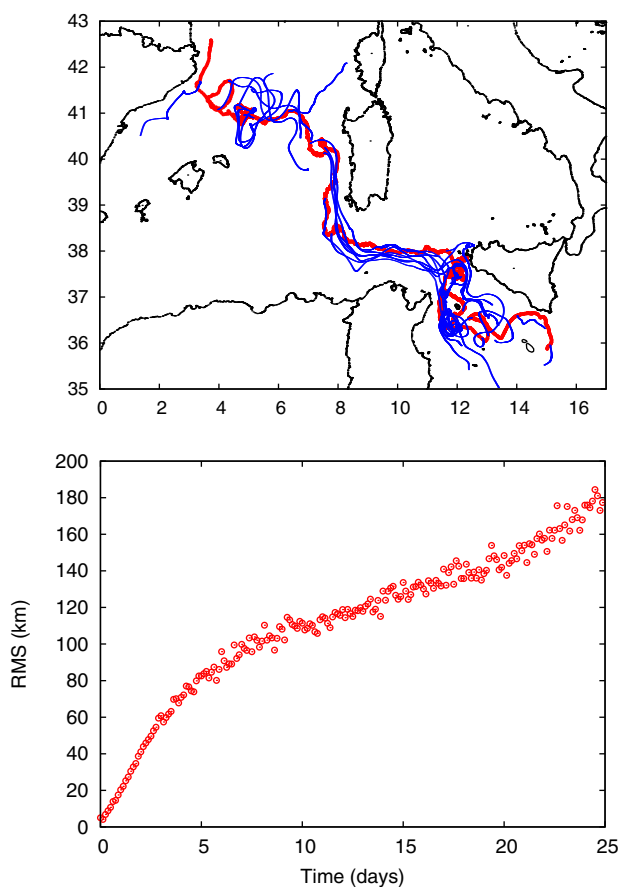
PALATELLA ET AL.   1318

As a final note, we would like to observe that the LTI, in principle, could also be exploited as additional information into multivariate models of anchovy population dynamics, together with standard predictors like temperature, chlorophyll, nutrients, and other indicators.

Appendix A: On the Error Growth Between Model and Drifter Trajectories

We present here some results about a reliability test we have performed on the MFS model, in relation to the Lagrangian simulations. We would like to stress that we limit ourselves to estimate how fast a numerical trajectory departs on average from a real drifter track, leaving a more detailed and exhaustive analysis of Lagrangian predictability to future work.

We consider a 6 month ocean drifter track as reference trajectory. The drifter data are provided by the ARGO program data catalog. The drifter WMO is 81855 and the datafile is available at http://www.ifremer.fr/co/co05010502/co_buoy_latex_61855C.csv. The chosen reference trajectory samples the Mediterranean Sea surface (at -15 m), along the path connecting the Gulf of Lions to the Sicily Channel (Figure A1, top). We divide the drifter trajectory in 5 day segments and, then, we take all segment starting points as initial conditions for a set of numerical trajectories that evolve with the MFS model velocities (with no subgrid parameterization). Numerical drifter trajectories describe neutrally buoyant tracers released at $z = -15$m evolving for a 25 day period. Within the experimental resolution error, all numerical trajectories have initial conditions lying on the drifter trajectory, and each of them generally tends to quickly depart from the drifter reference track because of the differences between the model velocity field and the actual marine circulation. Note that we are reducing, as much as possible, the sensitivity to the initial conditions of the MFS model by letting the numerical drifters begin their evolution from points located on the ocean drifter track; in this way, we isolate the contribution to the error growth due, at least initially, to the difference between simulated and actual dynamics.

In Figure A1 (bottom), we report the root mean square (RMS) separation of the $N = 32$ numerical trajectories from the reference track as a function of time. We note the presence of two characteristic time scales: one of the order of a few days, describing the fastest error growth for separations up to 40–50 km; the second of the order of one month, describing the slowest error growth on scales larger than 50 km. The first characteristic time and the associated separation scale correspond to the missing (or coarsely resolved) mesoscale components of the MFS model. The slowest error growth

Figure A1. (top) Comparison between the 61855 WMO buoyant drifter path (downloaded from the ARGO project website) (red line) and 32 model trajectories (blue lines), which have initial conditions along the drifter trajectory, starting every 5 days. The numerical trajectories evolve using the MFS model velocity field from 2010/09/19 to 2011/02/28. (bottom) Root-mean-square (RMS) error between drifter and model trajectories. The double slope behavior indicates the presence of two regimes having very distinct growth rate.

regime, on the other hand, having a characteristic time of the order of 1 month, would be relative to the action of nonlinear structures of the velocity field having size $\simeq 100\text{km}$ or larger, which are instead resolved with great accuracy by the MFS model, also thanks to the data assimilation procedures. On large separation scales, in the slow error growth regime, the differences between model and actual marine circulation tend to decrease, and the predictability of the Lagrangian trajectories depends, essentially, on the intrinsic chaoticity of the large-scale flow.

We conclude that an estimate of the trajectory uncertainty after 10 days of Lagrangian simulation using the MFS fields is of the order of 100 km, i.e., less than the size of the tracer spatial distribution as can be seen in the movie files given as supporting information. Thus, the error on an individual trajectory is less than the statistical error of the ensemble of trajectories considered.

Appendix B: Test Case: Meandering Jet Model

Let us consider a 2-D meandering jet model (Figure B1), as a prototype of the AIS system in the Sicily Channel. We start from a stream function Ψ of the form [*Bower*, 1991; *Samelson*, 1992; *Rogerson et al.*, 1999]:

$$\Psi = \tanh \frac{y - B_0 \cos(kx)}{\sqrt{1 + B_0^2 k^2 \sin^2(kx)}} - cy, \tag{B1}$$

where x and y are the spatial coordinates of a fluid particle, $k = 2\pi/l_0$ is the wave number, and l_0 is the spatial wavelength of the current system, B_0 gives the amplitude of the meanders, the term in the denominator of equation (B1) defines the width of the jet and c is a counter-stream (westward) velocity of the retrograde flow far from the central eastward flowing current. We thus derive the two velocity field components (u, v) as

$$u = \frac{\partial \Psi}{\partial y} \quad \text{and} \quad v = -\frac{\partial \Psi}{\partial x}. \tag{B2}$$

As a direct consequence of (B2), the divergence of the velocity field is necessarily null, i.e., $\partial u/\partial x + \partial v/\partial y \equiv 0$. The Lagrangian equations for a passive particle trajectory are therefore

$$\frac{dx}{dt} = u \quad \text{and} \quad \frac{dy}{dt} = v. \tag{B3}$$
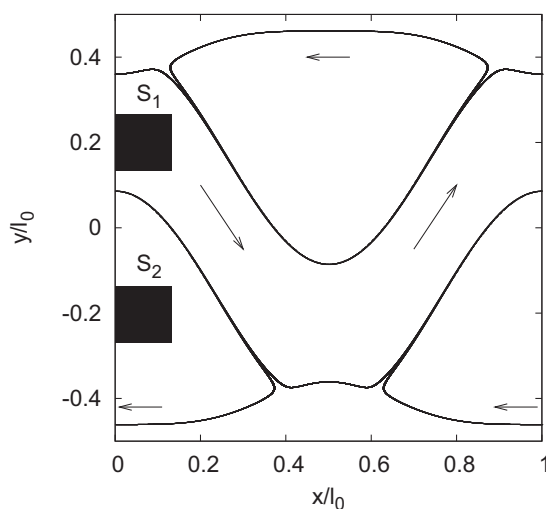
Figure B1. Spawning areas (black squares) in the Lagrangian simulations with the meandering jet model: S_1, inside the jet; S_2, inside a recirculating cell. The jet flows eastward while the northern (southern) circulating cells have anticlockwise (clockwise) rotation. The separatrices are the boundary lines between open and closed motions.

We define τ_a as the advective time scale of the flow, i.e., the minimum time that a particle in the middle of the jet takes to travel one spatial wavelength l_0 eastward. In the absence of an explicit time dependence of the stream function, the flow is steady and particle trajectories coincide with the Ψ isolines. In such a case, the initial positions of a set of particles completely determine their transport properties over a given spatial scale: referring to Figure B1, particles initially located inside the current (open streamlines) travel eastward (downstream) within the current and without bounds, while particles initially located
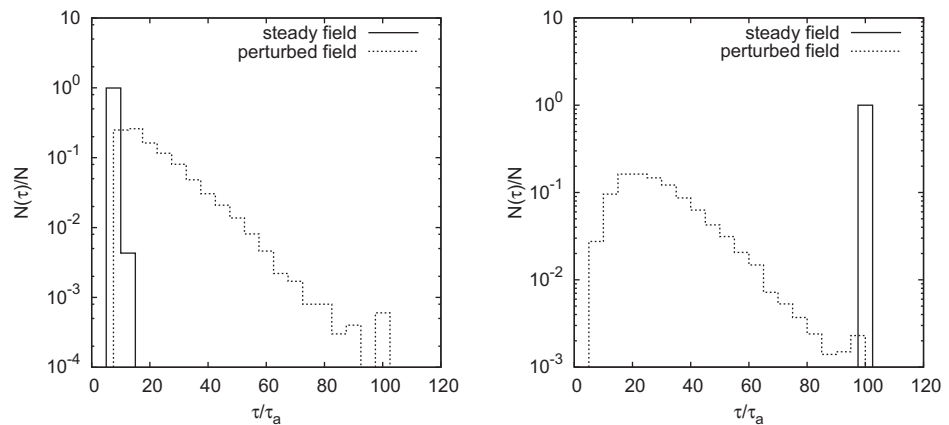
Figure B2. Lin-log plot of the normalized histograms of the first arrival time τ at a target placed at distance $I=5l_0$ along the x axis; $N(\tau)$ is the number of individuals arriving at time τ; and $N=10^4$ is the size of the ensemble. Spawning areas: (left) S_1; (right) S_2 (see Figure B1). The advective time τ_a is used as time unit for τ; the maximum waiting time is set to $T_w=10^2\tau_a$. For both the steady and the chaotic cases, the last bin contains the number of individuals that do not arrive at the target within the maximum waiting time.

inside a lateral vortex (closed streamlines) remain confined therein at all times. The flow is therefore separated into regions of qualitatively different dynamics by material lines (separatrices) that cannot be crossed. Chaotic trajectories, instead, can be generated by replacing B_0 with $B(t)$ defined as

$$B(t)=B_0+\varepsilon \cdot \cos(\omega t). \tag{B4}$$

This term induces a periodic oscillation of the meanders, with period $T_p=2\pi/\omega$ and amplitude ε, around the mean value B_0. The values of the perturbation parameters, ω and ε, control the width of the chaotic layer where the trajectories display strong sensitivity to small perturbations with an overall positive maximum Lyapunov exponent [Ott, 2002]. When the system is time dependent the separatrices change over time, so in this case transport barriers are no longer persistent.

In particular, keeping ω fixed, the amplitude ε can be varied from a weakly chaotic regime, in which chaos is confined in a thin layer around the separatrices of the flow, to a strong chaotic regime, in which any subset of the spatial domain contains chaotic motions. Therefore, in terms of Lagrangian transport, the effects of chaos result to be of primary importance for the mixing properties of the flow on large scales [Cencini et al., 1999; Lacorata et al., 2003]. In the meandering jet model (Figure B1), two virtual "spawning areas," containing $N=10^4$ individuals, are located in two dynamically different regions: one inside the jet, labeled S_1, and the other one inside a recirculating cell, labeled S_2. An imaginary target is placed at a distance $I=5l_0$, measured along the x axis; the first arrival time τ at the target position is then computed for all individuals, with an upper limit of a maximum waiting time interval $T_w \gg \tau_a$. For all those individuals that do not hit the target, the arrival time is conventionally set equal to the maximum waiting time, $\tau=T_w$.

In Figure B2, the distribution $N(\tau)$ of the first arrival time τ for the steady case, $\varepsilon=0$, is compared to that of the perturbed case, $\varepsilon \simeq 0.05l_0$ and $T_p=\tau_a$, for each of the two spawning areas. The role of chaos in the trajectories is reflected in change of shape of the distribution $N(\tau)$. In the steady case, all individuals released within the spawning area S_1, i.e., the jet, reach the target in a short time, much smaller than T_w: hence, the distribution $N(\tau)$ is very narrow, and peaks at short times (Figure B2, left). Differently, all individuals released inside a recirculating cell, spawning area S_2, never escape from there (Figure B2, right). In the chaotic case, the probability to observe "anomalous" behaviors, i.e., arrival time distribution with large tails, becomes nonzero. This happens for both spawning areas, in our model.

It is worth noticing that from the Eulerian point of view, the time-dependent velocity fields—e.g., sampled every period T_p—would look like the steady one, i.e., the time oscillating field (with $\varepsilon \neq 0$) and the steady

field (with $\varepsilon = 0$) would give exactly the same velocity pattern. On the contrary, particle transport at all scales, even over distances significantly larger than the meander wavelength, is strongly affected by the presence of Lagrangian chaos.

References

Basilone, G., A. Bonanno, B. Patti, S. Mazzola, M. Barra, A. Cuttitta, and R. McBride (2013), Spawning site selection by European anchovy (Engraulis encrasicolus) in relation to oceanographic conditions in the Strait of Sicily, *Fish. Oceanogr.*, *22*, 329–323.

Bec, J., L. Biferale, A. Lanotte, A. Scagliarini, and F. Toschi (2010), Turbulent pair dispersion of inertial particles, *J. Fluid Mech.*, *645*, 497–528.

Bees, M. (1998), Planktonic communities and chaotic advection in dynamical models of Langmuir circulation, *Appl. Sci. Res.*, *59*, 141–158.

Boffetta, G., A. Celani, A. Crisanti, and A. Vulpiani (1999), Pair dispersion in synthetic fully developed turbulence, *Phys. Rev. E*, *60*, 6734–6741.

Borja, A., A. Uriarte, J. Egana, L. Motos, and V. Valencia (1998), Relationships between anchovy (Engraulis encrasicolus) recruitment and environment in the Bay of Biscay (1967–1996), *Fish. Oceanogr.*, *7*, 375–380.

Bower, A. S. (1991), A simple kinematic mechanism for mixing fluid parcels across a meandering jet, *J. Phys. Oceanogr.*, *21*, 173–180.

Brickman, D., and P. C. Smith (2002), Lagrangian stochastic modeling in coastal oceanography, *J. Atmos. Oceanic Technol.*, *19*, 83–99.

Buongiorno Nardelli, B., G. Larnicol, E. D'Acunzo, R. Santoleri, S. Marullo, and P. Y. Le Traon (2003), Near real time SLA and SST products during 2-years of MFS pilot project: Processing, analysis of the variability and of the coupled patterns, *Ann. Geophys.*, *21*, 103–121.

Cencini, M., G. Lacorata, A. Vulpiani, and E. Zambianchi (1999), Mixing in a meandering jet: A Markovian approximation, *J. Phys. Oceanogr.*, *29*, 2578–2594.

Charney, J. (1971), Geostrophic turbulence, *J. Atmos. Sci.*, *28*, 1087–1095.

Ciappa, A. C. (2009), Surface circulation patterns in the Sicily Channel and Ionian Sea as revealed by MODIS chlorophyll images from 2003 to 2007, *Cont. Shelf Res.*, *29*, 2099–2109.

Cowen, R. K., K. M. M. Lwiza, S. Sponaugle, C. B. Paris, and D. B. Olson (2000), Connectivity of marine populations: Open or closed?, *Science*, *287*, 857–859.

Crisanti, A., M. Falcioni, G. Paladin, and A. Vulpiani (1991), Lagrangian chaos: Transport, mixing and diffusion in fluids, *Riv. Nuovo Cim.*, *14*, 1–80.

Cuttitta, A., et al. (2003), Anchovy egg and larval distribution in relation to biological and physical oceanography in the Strait of Sicily, *Hydrobiologia*, *503*, 117–120.

Dobricic, S., and N. Pinardi (2008), An oceanographic three-dimensional variational data assimilation scheme, *Ocean Modell.*, *22*, 89–105.

Durham, W. M., E. Climent, M. Barry, F. De Lillo, G. Boffetta, M. Cencini, and R. Stocker (2013), Turbulence drives microscale patches of motile phytoplankton, *Nat. Commun.*, *4*, 2148, doi:10.1038/ncomms3148.

Font, J., J. Salat, and J. Tintoré (1988), Permanent features of the circulation in the Catalan Sea, in *Oceanographie Pélagique Méditerranéenne, Oceanol. Acta, 9*, edited by H. J. Minas and P. Nival, Centre national de la recherche scientifique, Institut français de recherche pour l'exploitation de la mer. Paris, pp. 51–57.

Fox-Kemper, B., and R. Ferrari (2008), Parameterization of mixed layer eddies. Part II: Prognosis and impact, *J. Phys. Oceanogr.*, *38*, 1166–1179.

Fox-Kemper, B., R. Ferrari, and R. W. Hallberg (2008), Parameterization of mixed layer eddies. Part I: Theory and diagnosis, *J. Phys. Oceanogr.*, *38*, 1145–1165.

Fox-Kemper, B., G. Danabasoglu, R. Ferrari, S. M. Griffies, R. W. Hallberg, M. M. Holland, M. E. Maltrud, S. Peacock, and B. L. Samuels (2011), Parameterization of mixed layer eddies. III: Implementation and impact in global ocean climate simulations, *Ocean Modell.*, *39*, 61–78.

Frisch, U. (1995), *Turbulence: The Legacy of A. N. Kolmogorov*, 296 pp., Cambridge Univ. Press, N. Y.

Garcia, A., and I. Palomera (1996), Anchovy early life history and its relation to its surrounding environment in the Western Mediterranean basin, *Sci. Mar.*, *60*, 155–166.

Garcia-Lafuente, J., A. Garcia, S. Mazzola, L. Quintanilla, A. Delgado, A. Cuttita, and B. Patti (2002), Hydrographic phenomena influencing early life stages of the Sicilian Channel anchovy, *Fish. Oceanogr.*, *11*, 31–44.

Grilli, F., and N. Pinardi (1998), The computation of Rossby radii of deformation for the Mediterranean Sea, *MTP News*, *6*, 4.

Hutchings, L., et al. (1998), Multiple factors affecting South African anchovy recruitment in the spawning, transport and nursery areas, *S. Afr. J. Sci.*, *19*, 211–225.

LaCasce, J. H. (2008), Statistics from Lagrangian observations, *Prog. Oceanogr.*, *77*, 1–29.

Lacorata, G., R. A. Pasmanter, and A. Vulpiani (2003), Markov-chain approach to a process with long-time memory, *J. Phys. Oceanogr.*, *33*, 293–298.

Lacorata, G., A. Mazzino, and U. Rizza (2008), A 3D chaotic model for subgrid turbulent dispersion in large-eddy simulations, *J. Atmos. Sci.*, *65*, 2389–2401.

Lermusiaux, F. P. J. (1999), Estimation and study of mesoscale variability in the strait of Sicily, *Dyn. Atmos. Oceans*, *29*, 255–303.

Lermusiaux, P. F. J., and A. R. Robinson (2001), Features of dominant mesoscale variability, circulation patterns and dynamics in the Strait of Sicily, *Deep Sea Res., Part I*, *48*, 1953–1997.

Lloret, J., I. Palomera, J. Salat, and I. Sole (2004), Impact of freshwater input and wind on landings of anchovy (Engraulis encrasicolus) and sardine (Sardina pilchardus) in shelf waters surrounding the Ebre (Ebro) River delta (north-western Mediterranean), *Fish. Oceanogr.*, *13*, 102–110.

Malanotte-Rizzoli, P., and A. R. Robinson (1994), *Ocean Processes in Climate Dynamics: Global and Mediterranean Examples*, 464 pp., Kluwer Acad., Dordrecht, Netherlands.

Mariani, P., B. R. MacKenzie, D. Iudicone, and A. Bozec (2010), Modelling retention and dispersion mechanisms of bluefin tuna eggs and larvae in the northwest Mediterranean Sea, *Prog. Oceanogr.*, *86*, 45–48.

Marullo, S., R. Santoleri, D. Ciani, P. Le Borgne, S. Péré, N. Pinardi, M. Tonani, and G. Nardone (2013), Combining model and geostationary satellite data to reconstruct the hourly SST field over the Mediterranean Sea, *Remote Sens. Environ.*, doi:10.1016/j.rse.2013.11.001, in press.

Mazzola, S., A. Garcia, and J. Garcia-lafuente (2002), The Sicilian Channel anchovy fishery and the underlying oceanographic and biological processes conditioning their inter annual fluctuations, DG XIV, MED98-070, Final Report, 268 pp.

Napolitano, E., G. Sannino, V. Artale, and S. Marullo (2003), Modeling the baroclinic circulation in the area of the Sicily Channel: The role of stratification and energy diagnostics, *J. Geophys. Res.*, *108*(C7), 3230, doi:10.1029/2002JC001502.

Oddo, P., M. Adani, N. Pinardi, C. Fratianni, M. Tonani, and D. Pettenuzzo (2009), A nested Atlantic-Mediterranean Sea general circulation model for operational forecasting, *Ocean Sci.*, *5*, 461–473.

Olivar, M. P., J. Salat, and I. Palomera (2001), Comparative study of spatial distribution patterns of the early stages of anchovy and pilchard in the NW Mediterranean Sea, *Mar. Ecol. Prog. Ser.*, *217*, 111–120.

Ospina-Alvareza, A., C. Parada, and I. Palomera (2012a), Vertical migration effects on the dispersion and recruitment of European anchovy larvae: From spawning to nursery areas, *Ecol. Modell.*, *231*, 65–79.

Ospina-Alvareza, A., I. Palomera, and C. Parada (2012b), Changes in egg buoyancy during development and its effects on the vertical distribution of anchovy eggs, *Fish. Res.*, *117–118*, 86–95.

Ott, E. (2002), *Chaos in Dynamical Systems*, 492 pp., Cambridge Univ. Press, Cambridge, U. K.

Ottino, J. M. (1989), *The Kinematics of Mixing: Stretching, Chaos and Transport*, 364 pp., Cambridge Univ. Press, Cambridge, U. K.

Palomera, I., M. P. Olivar, J. Salat, A. Sabatés, M. Coll, A. García, and B. Morales-Nin (2007), Small pelagic fish in the NW Mediterranean Sea: An ecological review, *Prog. Oceanogr.*, *74*, 377–396.

Polton, J. A., and S. E. Belcher (2007), Langmuir turbulence and deeply penetrating jets in an unstratified mixed layer, *J. Geophys. Res.*, *112*, C09020, doi:10.1029/2007JC004205.

Poulain, P. M., and E. Zambianchi (2007), Surface circulation in the central Mediterranean Sea as deduced from Lagrangian drifters in the 1990s, *Cont. Shelf Res.*, *27*, 981–1001.

Quinci, E. M. (2011), Identificazione delle aree di deposizione e di nursery della acciuga europea (Engraulis encrasicolus) nel Canale di Sicilia, PhD dissertation, Universita' di Venezia Ca' Foscari, Dottorato di Ricerca in Scienze Ambientali, Ciclo XXIV.

Quintanilla, L. F., and A. Garcia (2001), Methodological, biological and environmental factors affecting the DEPM parameters variability in the Mediterranean anchovy, *Rapp. P. V. Reun. Comm. Int. Explor. Sci. Mer Mediter.*, *36*, 311.

Robinson, A. R., J. Sellschopp, A. Warn-Varnas, W. G. Leslie, C. J. Lozano, P. J. Harley Jr., L. A. Anderson, and P. J. F. Lermusiaux (1999), The Atlantic ionian stream, *J. Mar. Syst.*, *20*, 129–156.

Rogerson, A. M., P. D. Miller, L. J. Pratt, and C. K. R. T. Jones (1999), Lagrangian motion and fluid exchange in a barotropic meandering jet, *J. Phys. Oceanogr.*, *29*, 2635–2655.

Samelson, R. M. (1992), Fluid exchange across a meandering jet, *J. Phys. Oceanogr.*, *22*, 431–440.

Sawford, B. (2001), Turbulent relative dispersion, *Annu. Rev. Fluid Mech.*, *33*, 289–317.

Solomon, T. H., and J. P. Gollub (1988), Chaotic particle transport in time-dependent Rayleigh-Bénard convection, *Phys. Rev. A*, *38*, 6280–6286.

Somarakis, S., and N. Nikolioudakis (2007), Oceanographic habitat, growth and mortality of larval anchovy (Engraulis encrasicolus) in the northern Aegean Sea (eastern Mediterranean), *Mar. Biol.*, *152*, 1143–1158.

Sorgente, R., A. Olita, P. Oddo, L. Fazioli, and A. Ribotti (2011), Numerical simulation and decomposition of kinetic energy in the Central Mediterranean: Insight on mesoscale circulation and energy conservation, *Ocean Sci.*, *7*, 503–519.

Tonani, M., N. Pinardi, S. Dobricic, I. Pujol, and C. Fratianni (2008), A high-resolution free-surface model of the Mediterranean Sea, *Ocean Sci.*, *4*, 1–14.

Tonani, M., N. Pinardi, J. Pistoia, S. Dobricic, S. Pensieri, M. de Alfonso, and K. Nittis (2009), Mediterranean forecasting system: Forecast and analysis assessment through skill scores, *Ocean Sci.*, *5*, 649–660.

Vincenzi, D. (2013), Orientation of non-spherical particles in an axisymmetric random flow, *J. Fluid Mech.*, *719*, 465–487.